ACS APPLIED MATERIALS & INTERFACES

Research Article

www.acsami.org

Oligothiophene Interlayer Effect on Photocurrent Generation for Hybrid TiO_2/P3HT Solar Cells

Miquel Planells,[†,‡] Antonio Abate,[†,§] Henry J. Snaith,[*,§] and Neil Robertson[*,‡]

[‡]EaStCHEM − School of Chemistry, University of Edinburgh, Kings Buildings, Edinburgh EH9 3JJ, United Kingdom

[§]Department of Physics, University of Oxford, Oxford OX1 3PU, United Kingdom

Supporting Information

ABSTRACT: A series of conjugated 3-hexylthiophene derivatives with a cyanoacrylic acid group has been prepared with conjugation length from one up to five thiophene units (**1T**−**5T**). The UV−vis spectra, photoluminescence spectra, electrochemical data and DFT calculations show lowering of LUMO energies and red-shift of absorption into the visible as the thiophene chain length increases. TiO_2/P3HT solar cells were prepared with prior functionalization of the TiO_2 surface by **1T**−**5T** and studies include cells using undoped P3HT and using P3HT doped with H-TFSI. Without H-TFSI doping, photocurrent generation occurs from both the oligothiophene and P3HT. Doping the P3HT with H-TFSI quenches photocurrent generation from excitation of P3HT, but enables very effective charge extraction upon excitation of the oligothiophene. In this case, photocurrent generation increases with the light harvesting ability of **1T**−**5T** leading to a highest efficiency of 2.32% using **5T**. Overall, we have shown that P3HT can act in either charge generation or in charge collection, but does not effectively perform both functions simultaneously, and this illustrates a central challenge in the further development of TiO_2/P3HT solar cells.

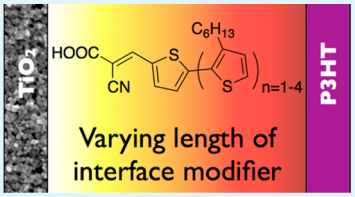

KEYWORDS: *Solar cells, oligothiophenes, P3HT, TiO_2, Dye-sensitized solar cells, organic semiconductors*

1. INTRODUCTION

In the past decade, impressive progress has been made in solar energy, both in experimental research and market activity.[1,2] In particular, photovoltaic cells made by solution processable materials are attracting great interest as an alternative to the established silicon technologies.[3] Though a number of different device concepts have been prepared by processing both organic and inorganic materials from solution,[3] the photoactive layer is always based on an interface between donor and acceptor semiconductors. One of the key challenges that restrict the choice of donor−acceptor combinations is the ability to simultaneously achieve an intimate contact, to guarantee an efficient charge separation at the interface, and a phase segregation to promote a percolation path for charge carrier transport to the electrodes. In fully organic devices for example, using conjugated polymers such as poly(3-hexylthiophene) (P3HT) as donor and organic small molecules such as fullerene derivatives as acceptor, the high chemical affinity of the two organic components facilitates the formation of a suitable interface, which results in efficient charge separation.[4−6] However, the same chemical affinity makes control and stabilization of the phase separation difficult, which is critical to generate percolation pathways for the charge extraction. Therefore, fully organic devices suffer from relatively low charge mobility and thermal instability of the phase segregation.[7] A potential solution to overcome these deficiencies is to combine organic and inorganic semiconductors.[8] As an example of such inorganic−organic hybrid solar cells, a transparent semiconductor such as TiO_2 acts as inorganic acceptor for the charges generated in the P3HT.[9,10] This device architecture is rooted in the well-known dye-sensitized solar cells (DSSCs) technology, with the difference that the P3HT is acting at the same time as light absorber, instead of the dye anchored on the TiO_2, and hole transporter, instead of the redox electrolyte.[11] The main advantage of this approach is the possibility to prepare a mesoporous TiO_2 electrode, which works as scaffold for the organic component and allows control and stabilization of the phase segregation.[11] In recent work, P3HT has been used as the hole conductor along with an additional light absorber in solid-state DSSCs, with power conversion efficiencies over 3%.[10,12] However, for these systems, almost all the photocurrent originates from light absorbed in the dye layer, and is not delivered from the P3HT. This literature indicates that electron transfer from photo-excited P3HT into TiO_2 does not occur very effectively. In this context, one of the key issues is the inherent incompatibility between the hydrophilic surface of the metal oxide and the hydrophobic nature of the conjugated polymer, which limits the intimate contact between the organic donor and the inorganic acceptor.[13] Several reports showed that the quality of this interface is crucial to achieve efficient charge separation in P3HT/TiO_2 hybrid systems.[14,15] We note here that the quality of the P3HT/TiO_2 interface is completely decoupled from the issue of the TiO_2 pore infiltration, which has been raised in previous studies to explain TiO_2/P3HT device performances.[12,16] Indeed, Canesi and co-workers demonstrated that,

Received: July 31, 2014
Accepted: September 18, 2014
Published: September 18, 2014

regardless of the pore filling fraction, the orientation and the packing of P3HT chains in contact with the TiO_2 surface are crucial to control the electronic coupling between the excited state energy levels in the polymer and the conduction band states in the oxide.[17] The same authors modified the TiO_2 surface with a molecular layer that drives local ordering of the polymer in contact with the surface, which enabled power conversion efficiency (PCE) above 1%. In another work, similar efficiency was reported by Grancini and co-workers, who observed efficient electron transfer from the photoexcited polymer to the TiO_2, functionalizing the metal oxide surface with fullerene derivatives.[7] In a different approach, the P3HT can be functionalized with carboxylic acid groups to directly anchoring the polymer to the TiO_2 and thus create a more intimate contact at TiO_2/P3HT interface.[16] However, despite the number of reports the effective operation of a functionalized P3HT/TiO_2 photoactive layer is quite poor.[13,15,18] The low device performances have been attributed to the presence of multiple anchoring groups on the same polymeric chain, which lowers the crystallinity of the polymer in contact with the TiO_2 and thus the possibility to achieve efficient charge separation.[17]

In this work, we report the synthesis and the characterization (electrochemical, optical and computational) for a series of conjugated oligo-3-hexylthiophenes (oligothiophene) derivatives, with a number of thiophene units from 1 to 5 (Figure 1).

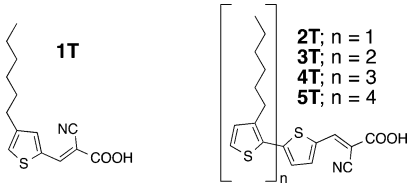

Figure 1. Molecular structures of the oligothiophene derivatives used in this study.

All the molecules are functionalized with a terminal cyanoacrylic acid group that allows anchoring the oligothiophenes on TiO_2 surface. We use those oligothiophene-functionalized TiO_2 to prepare TiO_2/P3HT solar cells and study the effect of the thiophene length on the device performance.

2. EXPERIMENTAL SECTION

2.1. Synthetic Procedure. *Materials.* All reagents were purchased from either Sigma-Aldrich or Alfa-Aesar and were used as received without further purification, except for 5-bromo-2-thiophenecarboxaldehyde, which was purified by silica plug in CH_2Cl_2 and *N*-Bromosuccinimide (NBS), which was recrystallized from water.

*Synthesis of 3-Hexylthiophene-5-carbaldehyde (**1**).* 3-Hexylthiophene (1 g, 5.9 mmol) was placed in a Schlenk tube with 15 mL of dry THF. The mixture was cooled down to −78 °C, stirred under N_2 and *n*-butyllithium 2.5 M in hexane (2.6 mL, 6.5 mmol) was added dropwise. Afterward, the reaction was warmed to 0 °C and stirred for 1 h. at 0 °C. Then, the mixture was cooled down again to −78 °C and DMF (550 μL, 7.1 mmol) was added dropwise. Finally, the reaction was warmed to room temp. and stirred for 3 h. The mixture was poured into a 100 mL 1% HCl aqueous solution and extracted with Et_2O (2 × 50 mL). The combined organic phases were joined together, washed with brine and dried over Na_2SO_4. After removing the solvent, the crude was purified by column chromatography (SiO_2, Hexanes up to Hexanes/EtOAc 20:1) to afford a mixture of isomers (85% 5-substituted/15% 2-substituted) as colorless oil (1.06 g, 91% yield). ^{1}H NMR (500 MHz, $CDCl_3$) δ_H: 9.87 (s, 1H); 7.60 (s, 1H); 7.36 (s, 1H); 2.64 (t, J = 7.7, 2H); 1.63 (m, 2H); 1.31 (m, 6H); 0.89 (t, J = 6.8, 3H). ^{13}C NMR (125 MHz, $CDCl_3$) δ_C: 183.2; 145.0; 143.8; 137.3; 130.6; 31.8; 30.6; 30.3; 29.0; 22.8; 14.3. MS EI (*m*/*z*) $[M]^+$ calcd for $C_{11}H_{16}OS$: 196.09164; found: 196.091333. Anal. Calcd for $C_{11}H_{16}OS$: C, 67.30; H, 8.22; found: C, 67.38; H, 8.14.

*Synthesis of (E)-2-Cyano-3-(3-hexylthiophen-5-yl)acrylic acid (**1T**).* **1** (700 mg, 3.5 mmol) and cyanoacetic acid (190 mg, 2.25 mmol) were placed in a Schlenk flask with 7 mL of EtOH. The mixture was stirred under N_2 and piperidine (750 μL, 17.5 mmol) was added. The reaction was heated up to 75 °C for 3 h. The mixture was then poured into 120 mL of aqueous HCl 1 M and the yellow precipitate collected by filtration. Pure product was obtained by washing the cake with H_2O, drying and then washing with few mL of cold hexane, giving the pure product as yellow solid (680 mg, 74% yield). ^{1}H NMR (500 MHz, $CDCl_3$) δ_H: 13.73 (br s, 1H); 8.44 (s, 1H); 7.86 (s, 1H); 7.81 (s, 1H); 2.60 (t, *J* = 7.6, 2H); 1.57 (m, 2H); 1.28 (m, 6H); 0.86 (t, *J* = 14.1, 3H). ^{13}C NMR (125 MHz, $CDCl_3$) δ_C: 163.5; 146.9; 144.1; 144.1; 140.2; 135.3; 131.8; 116.2; 98.5; 30.9; 29.7; 29.1; 28.2; 22.0; 13.9. MS EI (*m*/*z*) $[M]^+$ calcd for $C_{14}H_{17}NO_2S$: 263.09745; found: 263.09777. Anal. Calcd for $C_{20}H_{15}N$: C, 63.85; H, 6.51; N, 5.32; found: C, 63.68; H, 6.43; N, 5.22.

*Synthesis of Tributyl(3-hexylthiophen-2-yl) (**2**).* Mg turnings (530 mg, 22 mmol) were placed in a Schlenk flask with 10 mL of dry THF. The mixture was heated to 75 °C under N_2 and stirred for 3 h. The reaction was cooled down and then transferred via cannula under N_2 to a solution of 2-bromo-3-hexylthiophene (5 g, 20 mmol) in 10 mL of dry THF. The resulting mixture was cooled down to −78 °C and tributyltinchloride (6 mL, 22 mmol) was added dropwise. Then, the reaction was stirred overnight at room temperature under inert atmosphere. The crude was then poured into 200 mL of H_2O and extracted with 200 mL of hexane. The organic phase was dried over Na_2SO_4 and solvent removed, giving a pure product as yellowish oil (9.1 g, 99% yield) which was used without further purification. ^{1}H NMR (500 MHz, $CDCl_3$) δ_H: 7.54 (d, *J* = 4.6, 1H); 7.11 (d, *J* = 4.7, 1H); 2.61 (t, *J* = 8.0, 2H); 1.57 (m, 8H); 1.33 (m, 18H); 1.13 (m, 6H); 0.91 (m, 16H). ^{13}C NMR (125 MHz, $CDCl_3$) MS EI (*m*/*z*) $[M]^+$ calcd for $C_{22}H_{42}SSn$: 458.20237; found: 458.202735. Anal. Calcd for $C_{22}H_{42}SSn$: C, 57.78; H, 9.26; found: C, 57.62; H, 9.18.

*Synthesis of 3′-Hexyl-[2,2′-bithiophene]-5-carbaldehyde (**3**).* Tri(*o*-tolyl)phosphine (286 mg, 0.94 mmol) and tris-(dibenzylideneacetone)dipalladium (430 mg, 0.47 mmol) were placed in a Schlenk flask and dried under high vacuum for 30 min. Then, a solution of 5-bromo-2-thiophenecarboxaldehyde (3 g, 15.7 mmol) and **2** (7.2 g, 15.7 mmol) in dry and degassed toluene (63 mL) was transferred via cannula under Ar. The resulting solution was degassed again by pump-freeze technique and stirred at 90 °C overnight under N_2. Then, 70 mL of aqueous KF 1 M was added and stirred for 1 h. The organic fraction was collected and dried over Na_2SO_4, and the solvent was removed. The crude was purified by column chromatography (SiO_2, hexanes/5% EtOAc) to afford the product as yellow oil (3.01 g, 69% yield). ^{1}H NMR (500 MHz, $CDCl_3$) δ_H: 9.89 (s, 1H); 7.71 (d, *J* = 4.0, 1H); 7.28 (d, *J* = 5.2, 1H); 7.22 (d, *J* = 3.9, 1H); 6.98 (d, *J* = 5.2, 1H); 2.81 (t, *J* = 7.9, 2H); 1.65 (m, 2H); 1.38 (m, 2H); 1.31 (m, 4H); 0.88 (t, *J* = 7.1, 3H). ^{13}C NMR (125 MHz, $CDCl_3$) δ_C: 182.9; 146.9; 142.6; 142.3; 137.0; 130.9; 129.8; 129.8; 126.4; 126.0; 31.9; 30.6; 29.8; 29.4; 22.8; 14.3. MS EI (*m*/*z*) $[M]^+$ calcd for $C_{15}H_{18}OS_2$: 278.07936; found: 278.079133. Anal. Calcd for $C_{15}H_{18}OS_2$: C, 64.71; H, 6.52; found: C, 64.89; H, 6.54.

*Synthesis of (E)-2-Cyano-3-(3′-hexyl-[2,2′-bithiophen]-5-yl)-acrylic acid (**2T**).* **3** (200 mg, 0.72 mmol) and cyanoacetic acid (92 mg, 1.08 mmol) were placed in a Schlenk flask with 1.5 mL of EtOH. The mixture was stirred under N_2 and piperidine (350 μL, 3.6 mmol) was added. The reaction was heated up to 75 °C for 3 h. Then, the mixture was poured into 100 mL of aqueous HCl 1 M and the red precipitate was collected by filtration. Pure product was obtained by washing the cake with H_2O, giving a red solid (89 mg, 35% yield). ^{1}H NMR (500 MHz, $CDCl_3$) δ_H: 8.33 (s, 1H); 7.81 (d, *J* = 4.1, 1H); 7.32 (d, *J* = 5.2, 1H); 7.27 (d, *J* = 4.4, 1H); 6.99 (d, *J* = 5.2, 1H); 2.85 (t, *J* = 7.9, 2H); 1.67 (m, 2H); 1.41 (m, 2H); 1.31 (m, 4H); 0.89 (t, *J* = 6.9, 3H). ^{13}C NMR (125 MHz, $CDCl_3$) δ_C: 167.4; 148.6; 147.8; 143.0;

139.1; 134.8; 131.1; 129.6; 126.8; 126.7; 115.8; 96.6; 31.8; 30.6; 30.0; 29.4; 22.8; 14.3. MS EI (m/z): $[M]^+$ calcd for $C_{18}H_{19}NO_2S_2$: 345.08517; found: 345.08563. Anal. Calcd for $C_{18}H_{19}NO_2S_2$: C, 62.58; H, 5.54; N, 4.05; found: C, 62.47; H, 5.53; N, 3.97.

*Synthesis of 5′-Bromo-3′-hexyl-[2,2′-bithiophene]-5-carbaldehyde (**4**).* **3** (3 g, 10.7 mmol) was placed in a round-bottom flask with 33 mL of DMF and cooled down to 0 °C. NBS (2.28 g, 12.84 mmol) was added in small portions and the reaction was stirred overnight at room temp. Then, the mixture was poured into 200 mL of H_2O and extracted with 200 mL of Et_2O. The organic phase was washed with brine and dried over Na_2SO_4 and the solvent was removed. The crude was purified by column chromatography (SiO_2, Hexanes/5% EtOAc) to afford the product as yellow oil (2.38 g, 62% yield). ^{1}H NMR (500 MHz, $CDCl_3$) δ_H: 9.89 (s, 1H); 7.69 (d, J = 3.9, 1H); 7.15 (d, J = 3.9, 1H); 6.41 (s, 1H); 2.75 (t, J = 7.8; 2H); 1.62 (m, 2H); 1.37 (m, 2H); 1.30 (m, 4H); 0.87 (t, J = 7.0, 3H). ^{13}C NMR (125 MHz, $CDCl_3$) δ_C: 182.9; 145.2; 142.9; 142.8; 136.9; 133.5; 131.2; 126.7; 113.2; 31.8; 20.5; 29.7; 22.8; 22.7; 14.3. MS EI (m/z): $[M]^+$ calcd for $C_{15}H_{17}BrOS_2$: 355.98987; found: 355.990508. Anal. Calcd for $C_{15}H_{17}BrOS_2$: C, 50.42; H, 4.80; Found: C, 50.39; H, 4.91.

*Synthesis of 3′,3″-Dihexyl-[2,2′:5′,2″-terthiophene]-5-carbaldehyde (**5**).* Tri(*o*-tolyl)phosphine (121 mg, 0.4 mmol) and tris-(dibenzylideneacetone)dipalladium (183 mg, 0.2 mmol) were placed in a Schlenk flask and dried under a high vacuum for 30 min. Then, a solution of **4** (2.38 g, 6.7 mmol) and **2** (3.56 g, 3.6 mmol) in dry and degassed toluene (25 mL) was transferred via cannula under Ar. The resulting solution was degassed again by pump-freeze technique and stirred at 90 °C overnight under N_2. Then, 25 mL of aqueous KF 1 M was added and stirred for 1 h. The organic fraction was collected, dried over Na_2SO_4 and solvent removed. The crude was purified by column chromatography (SiO_2, Hexanes/5% EtOAc) to afford the product as yellow oil (2.01 g, 71% yield). ^{1}H NMR (500 MHz, $CDCl_3$) δ_H: 9.89 (s, 1H); 7.71 (d, J = 4.0, 1H); 7.23 (d, J = 4.0, 1H); 7.20 (d, J = 5.2, 1H); 6.98 (s, 1H); 6.94 (d, J = 5.2, 1H); 2.82 (t, J = 7.6, 2H); 2.78 (t, J = 7.8, 2H); 1.69 (m, 2H); 1.65 (m, 2H); 1.40 (m, 4H); 1.32 (m, 8H); 0.89 (m, 3H); 0.87 (m, 3H). ^{13}C NMR (125 MHz, $CDCl_3$) δ_C: 182.8; 146.5; 142.7; 142.3; 140.6; 137.1; 136.8; 130.5; 130.0; 129.4; 129.3; 126.1; 124.5; 31.9 (×2); 30.8; 30.5; 30.0; 29.6; 29.4 (×2); 22.8; 14.3 (×2). MS EI (m/z) $[M]^+$ calcd for $C_{25}H_{32}OS_3$: 444.16098; found: 444.161262. Anal. Calcd for $C_{25}H_{32}OS_3$: C, 67.52; H, 7.25; found: C, 67.39; H, 7.13.

*Synthesis of (E)-2-Cyano-3-(3′,3″-dihexyl-[2,2′:5′,2″-terthiophen]-5-yl)acrylic acid (**3T**).* **5** (250 mg, 0.56 mmol) and cyanoacetic acid (71 mg, 0.84 mmol) were placed in a Schlenk flask with 2.5 mL of EtOH. The mixture was stirred under N_2 and piperidine (275 μL, 2.8 mmol) was added. The reaction was heated up to 75 °C for 3 h. Then, the mixture was poured into a 100 mL of aqueous HCl 1 M and the formed red precipitate was collected by filtration. Pure product was obtained by washing the cake with H_2O, drying, stirring in EtO_2, and removal of the solvent, giving a deep-red solid (100 mg, 35% yield). ^{1}H NMR (500 MHz, $CDCl_3$) δ_H: 8.32 (s, 1H); 7.81 (d, J = 4.2, 1H); 7.27 (d, J = 4.2 1H); 7.21 (d, J = 5.3, 1H); 7.00 (s, 1H); 6.95 (d, J = 5.3, 1H); 2.85 (t, J = 7.8, 2H); 2.79 (t, J = 7.8, 2H); 1.71 (m, 2H); 1.64 (m, 2H); 1.45 (m, 2H); 1.39 (m, 2H); 1.32 (m, 8H); 0.90 (m, 3H); 0.89 (m, 3H). ^{13}C NMR (125 MHz, $CDCl_3$) δ_C: 167.2; 148.1; 147.5; 143.5; 140.8; 139.1; 137.6; 134.6; 130.5; 129.9; 129.5; 129.2; 126.4; 124.7; 116.0; 96.4; 31.9 (x2); 30.7; 30.4; 30.2; 29.6; 29.4 (×2); 22.8 (×2) 14.3 (×2). MS EI (m/z) $[M]^+$ calcd for $C_{28}H_{33}NO_2S_3$: 511.16679; found: 511.166823. Anal. Calcd for $C_{28}H_{33}NO_2S_3$: C, 65.71; H, 6.50; N, 2.74; found: C, 65.83; H, 6.57; N, 2.80.

*Synthesis of 5″-Bromo-3′,3″-dihexyl-[2,2′:5′,2″-terthiophene]-5-carbaldehyde (**6**).* **5** (2 g, 4.5 mmol) was placed in a round-bottom flask with 14 mL of DMF and cooled down to 0 °C. NBS (800 mg, 4.5 mmol) was added in small portions and the reaction was stirred overnight at room temp. Then, the mixture was poured into 200 mL of H_2O and extracted with 200 mL of Et_2O. The organic phase was washed with brine and dried over Na_2SO_4, and the solvent was removed. The crude was purified by column chromatography (SiO_2, Hexanes/5% EtOAc) to afford the product as yellow oil (2 g, 85% yield). ^{1}H NMR (500 MHz, $CDCl_3$) δ_H: 9.89 (s, 1H); 7.71 (d, J = 4.0, 1H); 7.22 (d, J = 4.0, 1H); 6.91 (s, 1H); 6.90 (s, 1H); 2.80 (t, J = 7.9, 2H); 2.71 (t, J = 7.9, 2H); 1.67 (m, 2H); 1.61 (m, 2H); 1.41 (m, 2H); 1.37 (m, 2H); 1.31 (m, 8H); 0.89 (m, 6H). ^{13}C NMR (125 MHz, $CDCl_3$) δ_C: 182.8; 146.1; 142.6; 142.5; 141.1; 137.0; 135.3; 133.1; 131.5; 129.9; 129.6; 126.4; 111.3; 31.8 (×2); 30.7; 30.4; 29.9; 29.5; 29.4; 29.3; 22.8 (×2); 14.3 (x2). MS EI (m/z) $[M]^+$ calcd for $C_{25}H_{31}BrOS_3$: 522.07149; found: 522.071220. Anal. Calcd for $C_{25}H_{31}BrOS_3$: C, 57.35; H, 5.97; found: C, 60.44; H, 6.27.

*Synthesis of 3′,3″,3‴-Trihexyl-[2,2′:5′,2″:5″,2‴-quaterthiophene]-5-carbaldehyde (**7**).* Tri(*o*-tolyl)phosphine (69 mg, 0.23 mmol) and tris(dibenzylideneacetone)dipalladium (105 mg, 0.115 mmol) were placed in a Schlenk flask and dried under a high vacuum for 30 min. Then, a solution of **6** (2 g, 3.82 mmol) and **2** (1.92 g, 4.2 mmol) in dry and degassed toluene (15 mL) was transferred via cannula under Ar. The resulting solution was degassed again by pump-freeze technique and stirred at 90 °C overnight under N_2. Then, 10 mL of aqueous KF 1 M was added and stirred for 1 h. The organic fraction was collected, dried over Na_2SO_4 and solvent removed. The crude was purified by column chromatography (SiO_2, Hexanes/5% EtOAc) to afford the product as orange oil that solidifies at −20 °C (1.66 g, 71% yield). ^{1}H NMR (500 MHz, $CDCl_3$) δ_H: 9.89 (s, 1H); 7.71 (d, J = 4.0, 1H); 7.24 (d, J = 4.0, 1H); 7.17 (d, J = 5.1, 1H); 7.00 (s, 1H); 6.95 (s, 1H); 6.94 (d, J = 5.1, 1H); 2.83 (t, J = 7.8, 2H); 2.78 (t, J = 7.8, 4H); 1.69 (m, 6H); 1.42 (m, 6H); 1.33 (m, 12H); 0.69 (m, 9H). ^{13}C NMR (125 MHz, $CDCl_3$) δ_C: 182.7; 146.5; 142.7; 142.3; 140.8; 140.1; 137.1; 136.5; 135.1; 130.5; 130.4; 128.8; 129.4; 129.1; 129.0; 126.0; 124.5; 31.9 (x3); 30.8; 30.6; 30.5; 30.0; 29.7; 29.5; 29.4 (×3); 22.8 (×3); 14.3 (×3). MS EI (m/z) $[M]^+$ calcd for $C_{35}H_{46}OS_4$: 610.24260; found: 610.242491. Anal. Calcd for $C_{35}H_{46}OS_4$: C, 68.80; H, 7.59; found: C, 68.98; H, 7.43.

*Synthesis of (E)-2-Cyano-3-(3′,3″,3‴-trihexyl-[2,2′:5′,2″:5″,2‴-quaterthiophen]-5-yl)acrylic acid (**4T**).* **7** (611 mg, 1 mmol) and cyanoacetic acid (130 mg, 1.5 mmol) were placed in a Schlenk flask with 4 mL of EtOH. The mixture was stirred under N_2 and piperidine (500 μL, 5 mmol) was added. The reaction was heated up to 75 °C for 5 h. The mixture was then poured into a 100 mL of aqueous HCl 1 M and the red-dark precipitate was centrifuged 15 min at 4400 rpm. The precipitate was dissolved in $CHCl_3$, dried over Na_2SO_4, giving the pure product as deep-red solid (626 mg, 92% yield). ^{1}H NMR (500 MHz, $CDCl_3$) δ_H: 8.30 (s, 1H); 7.80 (d, J = 4.1, 1H); 7.27 (d, J = 4.1, 1H); 7.17 (d, J = 5.2, 1H); 7.01 (s, 1H); 6.95 (s, 1H); 6.93 (d, J = 5.2, 1H); 2.86 (t, J = 7.9, 2H); 2.79 (m, 4H); 1.69 (m, 6H); 1.43 (m, 6H); 1.34 (m, 12H); 0.91 (m, 9H). ^{13}C NMR (125 MHz, $CDCl_3$) δ_C: 168.3; 148.3; 147.5; 143.7; 141.1; 140.1; 139.4; 137.4; 135.4; 134.5; 130.4 (×2); 129.7; 129.2 (×2); 129.1; 126.3; 124.1; 115.9; 96.1; 31.9 (×3); 30.8; 30.6; 30.4; 30.3; 29.8; 29.6; 29.5 (×3); 22.8 (×3); 14.3 (×3). MS EI (m/z) $[M]^+$ calcd for $C_{38}H_{47}NO_2S_4$: 677.24841; found: 677.248566. Anal. Calcd for $C_{38}H_{47}NO_2S_4$: C, 67.31; H, 6.99; N, 2.07; found: C, 67.22; H, 7.03; N, 2.17.

*Synthesis of 5‴-Bromo-3′,3″,3‴-trihexyl-[2,2′:5′,2″:5″,2‴-quaterthiophene]-5-carbaldehyde (**8**).* **7** (1 g, 1.64 mmol) was placed in a round-bottom flask with 8 mL of DMF and cooled down to 0 °C. NBS(291 mg, 1.64 mmol) was added in small portions and the reaction was stirred overnight at room temp. Then, the mixture was poured into 200 mL of H_2O and extracted with 200 mL of Et_2O. The organic phase was washed with brine and dried over Na_2SO_4, and the was solvent removed. The crude was purified by column chromatography (SiO_2, hexanes/5% EtOAc) to afford the product as orange oil (1.04 g, 92% yield). ^{1}H NMR (500 MHz, $CDCl_3$) δ_H: 9.89 (s, 1H); 7.71 (d, J = 4.0, 1H); 7.24 (d, J = 4.0, 1H); 6.99 (s, 1H); 6.89 (s, 1H); 6.88 (s, 1H); 2.82 (t, J = 7.8, 2H); 2.77 (t, J = 7.8, 2H); 2.71 (t, J = 7.8, 2H); 1.68 (m, 4H); 1.61 (m, 2H); 1.32 (m, 18H); 0.89 (m, 9H). ^{13}C NMR (125 MHz, $CDCl_3$) δ_C: 182.8; 146.3; 142.7; 142.4; 140.8; 140.6; 137.1; 136.1; 133.6; 132.9; 131.9; 130.4; 129.6; 129.4; 129.3; 126.1; 110.8; 31.8 (×3); 30.7; 30.6; 30.4; 30.0; 29.6; 29.4 (×3); 29.3; 22.8 (×3); 14.3 (x3). MS EI (m/z) $[M]^+$ calcd for $C_{35}H_{45}BrOS_4$: 688.15311; found: 688.153678. Anal. Calcd for $C_{35}H_{45}BrOS_4$: C, 60.93; H, 6.57; found: C, 60.83; H, 6.46.

*Synthesis of 3′,3″,3‴,3⁗-Tetrahexyl-[2,2′:5′,2″:5″,2‴:5‴,2⁗-quinquethiophene]-5-carbaldehyde (**9**).* Tri(*o*-tolyl)phosphine (28

mg, 90 μmol) and tris(dibenzylideneacetone)dipalladium (41 mg, 45 μmol) were placed in a Schlenk flask and dried under a high vacuum for 30 min. Then, a solution of **8** (1.04 g, 1.50 mmol) and **2** (760 mg, 1.66 mmol) in dry and degassed toluene (6 mL) was transferred via cannula under Ar. The resulting solution was degassed again by pump-freeze technique and stirred at 90 °C overnight under N_2. Then, 10 mL of aqueous KF 1 M was added and stirred for 1 h. The organic fraction was collected and dried over Na_2SO_4, and solvent was removed. The crude was prepurified by a silica plug ($CHCl_3$) and then column chromatography (SiO_2, hexanes/5% EtOAc) to afford the product as orange-red oil that solidifies at −20 °C (833 mg, 72% yield). ^{1}H NMR (500 MHz, $CDCl_3$) δ_H: 9.89 (s, 1H); 7.71 (d, J = 4.0, 1H); 7.24 (d, J = 4.0, 1H); 7.17 (d, J = 5.2, 1H); 7.01 (s, 1H); 6.97 (s, 1H); 6.97 (s, 1H); 6.93 (d, J = 5.2, 1H); 2.83 (t, J = 7.9, 2H); 2.78 (m, 6H); 1.69 (m, 8H); 1.42 (m, 8H); 1.33 (m, 16H); 0.90 (m, 12H). ^{13}C NMR (125 MHz, $CDCl_3$) δ_C: 182.7; 146.4; 142.8; 142.3; 140.8; 140.2; 139.9; 137.1; 136.4; 134.7; 134.6; 130.6; 130.4; 130.3; 129.8; 129.4; 129.1; 129.0; 128.8; 126.1; 123.9; 31.9 (×4); 30.9; 30.7 (×2); 30.5; 30.0; 29.7 (×2); 29.5; 29.4 (×4); 22.8 (×4); 14.3 (×4). MS EI (m/z) $[M]^+$ calcd for $C_{45}H_{60}OS_5$: 776.32422; found: 776.324025. Anal. Calcd for $C_{45}H_{60}OS_5$: C, 69.53; H, 7.78; found: C, 69.51; H, 7.77.

*Synthesis of (E)-2-Cyano-3-(3′,3″,3‴,3⁗-tetrahexyl-[2,2′:5′,2″:5″,2‴:5‴,2⁗-quinquethiophen]-5-yl)acrylic acid (**5T**).* **9** (200 mg, 0.26 mmol) and cyanoacetic acid (33 mg, 0.39 mmol) were placed in a Schlenk flask with 2 mL of EtOH. The mixture was stirred under N_2 and piperidine (130 μL, 1.30 mmol) was added. The reaction was heated up to 75 °C for 5 h. Then, the mixture was poured into 100 mL of aqueous HCl (1M) and extracted with Et_2O. The crude was purified by size exclusion chromatography (Biobeads S-X1, CH_2Cl_2) to afford the product as deep-red solid (118 mg, 54% yield). ^{1}H NMR (500 MHz, $CDCl_3$) δ_H: 8.32 (s, 1H); 7.82 (d, J = 4.4, 1H); 7.29 (d, J = 4.3, 1H); 7.17 (d, J = 5.2, 1H); 7.03 (s, 1H); 6.98 (s, 1H); 6.95 (s, 1H); 6.93 (d, J = 5.2, 1H); 2.87 (t, J = 7.8, 2H); 2.79 (m, 6H); 1.70 (m, 8H); 1.44 (m, 8H); 1.34 (m, 16H); 0.90 (m, 9H). ^{13}C NMR (125 MHz, $CDCl_3$) δ_C: 166.5; 148.0; 147.4; 143.5; 141.0; 140.2; 139.8; 139.1; 137.2; 134.9; 134.5; 134.4; 130.4; 130.2; 130.0; 129.5; 129.1; 129.0; 128.8; 128.7; 126.2; 123.7; 115.8; 95.8; 31.7 (x4); 30.7; 30.5; 30.4; 30.2; 30.1; 29.6; 29.5; 29.3; 29.2 (×4); 22.6 (×4); 14.1 (×4). MS EI (m/z) $[M]^+$ calcd for $C_{48}H_{61}NO_2S_5$: 843.33004; found: 843.330356. Anal. Calcd for $C_{48}H_{61}NO_2S_5$: C, 68.28; H, 7.28; N, 1.66; found: C, 68.16; H, 7.19; N, 1.62.

2.2. Methods. *Chemical Characterization.* ^{1}H and ^{13}C NMR spectra were recorded on Bruker Advance 500 spectrometer (500 MHz for ^{1}H and 125 MHz for ^{13}C). The deuterated solvents are indicated; chemical shifts, δ, are given in ppm, referenced to TMS, standardized by the solvent residual signal (^{1}H, ^{13}C). Coupling constants (J) are given in hertz (Hz). MS were recorded on ThermoElectron MAT 900 using electron impact (EI) ionization technique. Elemental analyses were carried out by Stephen Boyer at London Metropolitan University using a Carlo Erba CE1108 Elemental Analyzer.

Electrochemical Characterization. All cyclic voltammetry measurements were carried out in freshly distilled CH_2Cl_2 using 0.3 M $[TBA][PF_6]$ electrolyte in a three-electrode system, with each solution being purged with N_2 prior to measurement. The working electrode was a Pt disk. The reference electrode was Ag/AgCl and the counter electrode was a Pt rod. All measurements were made at room temp. using an μAUTOLAB Type III potentiostat, driven by the electrochemical software GPES. Cyclic voltammetry (CV) measurements used scan rates of 25, 50, 100, 200, and 500 mV/s. Square wave voltammetry (SWV) experiments were carried out at a step potential of 4 mV, a square wave amplitude of 25 mV and a square wave frequency of 15 Hz, giving a scan rate of 40 mV/s. Ferrocene was used as internal standard in each measurement.

Optical Characterization. Solution UV−visible absorption spectra were recorded using Jasco V-670 UV/vis/NIR spectrophotometer controlled using the SpectraManager software. Photoluminescence (PL) spectra were recorded with Fluoromax-3 fluorimeter controlled by the ISAMain software. All samples were measured in a 1 cm cell at room temp. with dichloromethane as a solvent. Concentration of 2×10^{-5} M and 5×10^{-6} M were used for UV/visible and PL, respectively.

Computational Details. The molecular structures were optimized first in vacuum without any symmetry constrains, followed by the addition of CH_2Cl_2 solvation via a conductor-like polarizable continuum model (C-PCM).[19] The presence of local minimum was confirmed by the absence of imaginary frequencies. All calculations were carried out using the Gaussian 09 program[20] with the Becke three parameter hybrid exchange, Lee−Yang−Parr correlation functional (B3LYP) level of theory. All atoms were described by the 6-31G(d) basis set. All structures were input and processed through the Avogadro software package.[21]

Solar Cells Fabrication. Solar cells were prepared following the procedure we previously reported.[22] All solvents used for device fabrication were reagent grade and anhydrous. FTO substrates (7 Ω/sq, Pilkington US) were etched with zinc powder and HCl (2 M aqueous solution) to give the desired electrode patterning. The substrates were cleaned with Hellmanex (2% by volume in water, Aldrich), deionized water, acetone, and ethanol. The last traces of organic residues were removed by 10 min oxygen plasma cleaning. The FTO sheets were subsequently coated with a compact layer of TiO_2 (about 70 nm) by aerosol spray pyrolysis deposition at 275 °C, using oxygen as the carrier gas and titanium diisopropoxide bis(acetylacetonate) as precursor. Films of 1.5 μm thick mesoporous TiO_2 were then deposited by screen-printing a commercial paste (Dyesol 18NR-T). The TiO_2 films were slowly heated to 500 °C and allowed to sinter for 30 min in air. Once cooled, the samples were immersed into a 15 mM $TiCl_4$ aqueous solution for 45 min at 70 °C and then heated to 500 °C for another sintering step of 45 min. After cooling to 70 °C, the substrates were immersed in a 500 μM solution of oligothiophene in 1:1 v:v mixture of acetonitrile and *tert*-butyl alcohol, for 30 min. After the TiO_2 functionalization, the films were rinsed in acetonitrile, the P3HT was applied by spin-coating at 1000 rpm for 45 s in air from solution (30 mg/mL in chlorobenzene).[17,23] Bis(trifluoromethanesulfonyl)imide (H-TFSI) was added in the P3HT solution prior to spinning as previously described where appropriate.[22] After drying overnight, back contacts were applied by thermal evaporation of 150 nm of silver.

Solar Cells Performance Characterization.[24] For measuring the device merit parameters, simulated AM 1.5 sunlight was generated with a class AAB ABET solar simulator calibrated to give simulated AM 1.5, 100 mW cm^{-2} irradiance, using an NREL-calibrated KG5 filtered silicon reference cell, with less than 1% mismatch factor; the current−voltage curves were recorded with a sourcemeter (Keithley 2400, USA). The solar cells were masked with a metal aperture defining the active area (0.12 cm^2) of the solar cells.

External Quantum Efficiency (EQE). Photovoltaic action spectra were measured (2400 Series SourceMeter, Keithley Instruments) with chopped monochromatic light incident which were biased with white light-emitting diodes (LED) at an equivalent solar irradiance of 100 mW·cm^{-2}. The monochromatic light intensity for the incident photon-to-electron conversion efficiency was calibrated with a UV-enhanced silicon photodiode. The solar cells were masked with a metal aperture to define the active area which was typically 0.12 cm^2 and measured in a light-tight sample holder to minimize any edge effects.

3. RESULTS AND DISCUSSION

3.1. Synthesis. The synthetic route used to obtain the oligothiophene series is shown in Scheme 1. Synthesis of **1T** was not straightforward, since the formylation at the 5-substituted position was not fully selective. **1** was obtained as an isomeric mixture in a 15:85 ratio between 2- and 5-substituted carbaldehydes (confirmed by ^{1}H NMR in the Supporting Information) and further separation was not possible by conventional purification techniques. However, by controlling carefully the reaction times, the 5-substituted carbaldehyde isomer reacted completely to **1T** whereas the 2-substituted isomer remained unaffected due to higher steric hindrance

Scheme 1. Synthetic procedure for the synthesis of oligothiophene series

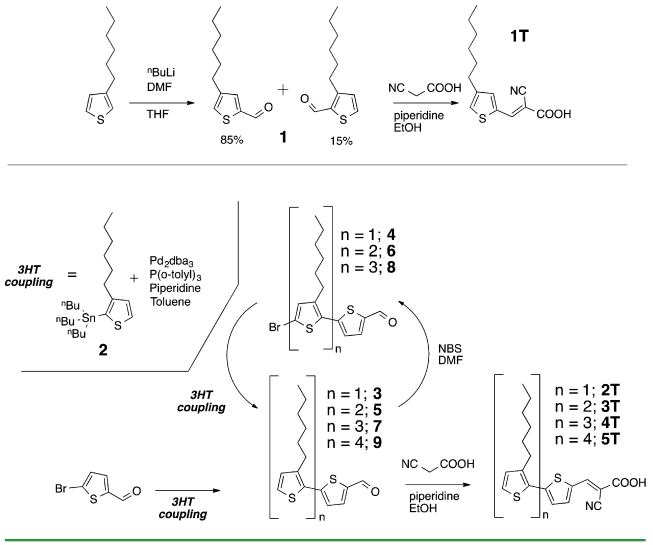

(confirmed by ^{1}H NMR in the Supporting Information). This allowed us to purify the mixture by simply washing the crude with neat hexane. For **2T** to **5T**, palladium catalyzed cross-coupling reactions were carried out in order to systematically increase the thiophene core chain length. In our case, we chose Stille coupling over Suzuki because higher yields were obtained. Then, selective bromination at the thiophene 5-position was attained by using NBS in dry DMF. Finally, the cyanoacrylic group was attached via Knoevenagel condensation for all molecules.

3.1. Optical Properties. Optical properties of our oligothiophene series were studied in dichloromethane solution. As expected, a systematic increment of the thiophene units led to red-shifted and more intense bands (Figure 2). This

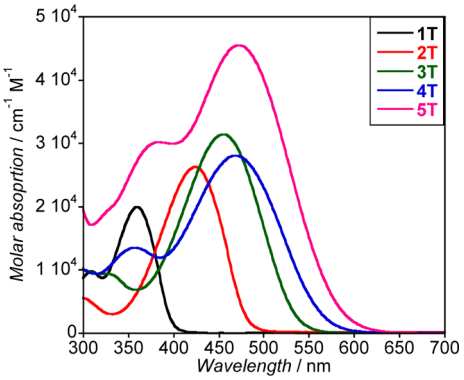

Figure 2. Absorbance spectra of oligothiophene molecules acquired at 5×10^{-5} M in CH_2Cl_2. We should note that the **5T** absorption is for its aggregated form at this concentration (see the Supporting Information).

is due to the extra conjugation and electron delocalization within the thiophene backbone, which reduces the molecular HOMO–LUMO gap. Therefore, **1T** showed only absorption in the UV region, whereas visible absorption was attained after increasing the 3HT chain length, with a gradual red shift. In addition, we observed that the absorption spectral shape of **5T** was concentration dependent (see the Supporting Information). Interestingly, this behavior is not observed in any of the other oligothiophene materials reported in this study. We believe that at the working concentration range for optical studies (from 1×10^{-6} to 1×10^{-4} M), $\pi-\pi$ stacking interactions between molecules becomes significant after the addition of the fifth 3HT unit, but not before.

Photoluminescence (PL) was also studied in solution and is shown in Figure 3. In this case, no PL was observed for the

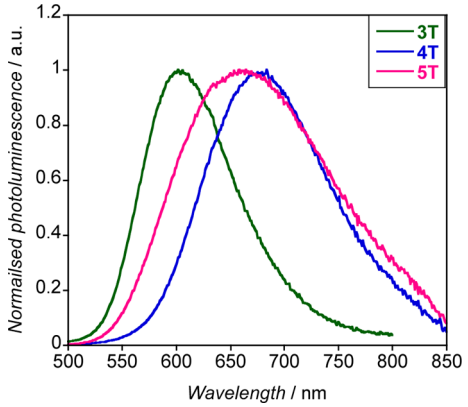

Figure 3. Photoluminescence (PL) spectra of emissive oligothiophene molecules acquired at 5×10^{-6} M CH_2Cl_2 solutions and excited at λ_{max}. **1T** and **2T** did not show PL.

smaller oligothiophene molecules (**1T** and **2T**); however, it was seen for the larger derivatives, covering the visible and even the near-IR region with a very large Stokes-shift (from 4500 to 6500 cm^{-1}).[25] The optical gap was extracted by the absorption onset and all optical data are shown in Table 1.

3.2. Electrochemistry. Electrochemical properties for the oligothiophene series were evaluated by cyclic (CV) and square-wave (SWV) voltammetries and referenced to ferrocene (Figure 4 and the Supporting Information). Both oxidation and reduction processes can be observed for the whole series, except for **1T**. In this case, the oxidation potential lies beyond the solvent electrochemical window. We observe a clear trend in the oxidation potentials as we increase the thiophene core length. As expected, an increment in electron-rich substituents (i.e., addition of thiophene units) shifts the oxidation peaks to less positive potential and reduces the electrochemical gap between the first oxidation and first reduction potentials. Irreversible electrochemical traces were observed for **2T**, **3T**, and **4T** indicating that those molecules do not generate stable cations in solution on electrochemical time scales (1×10^{-1} to 1 s). However, those materials might work well in functional devices as the oxidized cation is regenerated by the hole transport material at much faster time scales (1×10^{-10} to 1×10^{-9} s), which it may prevent decomposition. On the other hand, it is notable that **5T** shows reversible electrochemical behavior, even in solution (see the Supporting Information).

For the reduction processes, we can see a slight shift to less negative potentials after increasing the thiophene chain length. This shift between molecules in the series is in general much smaller than that observed for the oxidation processes, and negligible for longer thiophene units. This is because the LUMO is localized mainly over both the cyanoacrylic moiety and its directly attached first thiophene unit, as shown later in the text by DFT calculations. Thus, the reduction processes is nearly independent of the thiophene chain length.

The gap obtained from electrochemical measurements follows the same trend as the optical gap, but is 0.2 to 0.4

dx.doi.org/10.1021/am5050532 | ACS Appl. Mater. Interfaces 2014, 6, 17226–17235

Table 1. Summary of Optical and Electrochemical Properties for the Oligothiophene Series Acquired in CH_2Cl_2 Solution

	λ_{max} (nm)	ε (cm^{-1} M^{-1})	λ_{em} (nm)	E_{gap}^{OPT} (eV)[a]	E_{OX} (V)[b]	E_{RED} (V)[b]	E_{gap}^{CV} (eV)[c]	$E_{gap}^{CV} - E_{gap}^{OPT}$
1T	360	21 700	n/o[d]	3.10	n/o	−2.20	n/a[e]	n/a
2T	425	28 250	n/o	2.58	+0.92	−2.04	2.90	0.38
3T	455	32 000	600	2.31	+0.66	− 1.95	2.50	0.30
4T	470	28 000	675	2.19	+0.50	−1.94	2.33	0.25
5T	436−472[f]	45 700	660	2.12	+0.39	−1.92	2.25	0.19

[a]Optical gap obtained from the absorption onset. [b]Obtained from the oxidation (reduction) peak onsets. [c]Electrochemical gap = $E_{OX} - E_{RED}$. [d]Not observed. [e]Not available. [f]Optical properties are concentration dependent (see the Supporting Information).

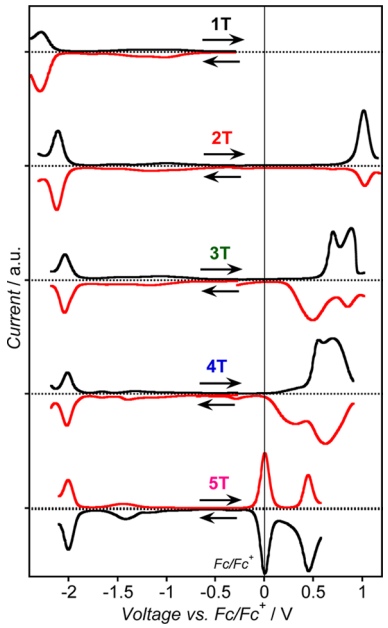

Figure 4. SWV of oligothiophene derivatives recorded in CH_2Cl_2 solution containing 0.3 M [TBA][PF_6] and referenced internally to ferrocene (showed in **5T** scan only). Arrows indicate the direction of scan. The small broad band located between −1.0 and −1.5 V for all samples has been attributed to the reduction of carboxylic protons.

eV larger. This is not unexpected, because the Coulombic exciton binding energy is not included in the electrochemical measurement.[26] In addition, we observed that the excition binding energy was reduced by increasing the thiophene chain length, indicating greater spatial separation of the electron−hole pair, in good agreement with the literature.[27]

3.3. Computational Studies. Hybrid DFT calculations were performed, using Gaussian 09, B3LYP/6-31G(d) level of theory, in order to shed light on the optical and electrochemical experimental results. After applying the solvent contribution via C-PCM, the computed values for the HOMO and LUMO energy levels were compared to experimental values obtained from electrochemistry measurements.

In this case and due to the nonfully reversible electrochemical nature of our oligothiophene molecules, we converted the electrochemically measured potentials (V) into energy levels versus vacuum (eV) with the following equation: $E_{HOMO/LUMO}$ (eV vs. vacuum) = −4.88 − $E_{OX/RED}$ (V vs. Fc/Fc^+).[28] As can be seen in Table 2, the computed values for E_{LUMO} are accurately predicted, showing an error of ±0.1 eV. In addition, there is not much variation among samples, as the LUMO electron density is (de)localized on the cyanoacrylic moiety and its adjacent thiophene only (Figure 5). This motif is present in the whole series and therefore we observe only a small shift in E_{LUMO}, in a good agreement with our electrochemical data.

Table 2. Theoretical and Experimental Values for HOMO and LUMO Energy Levels in eV vs Vacuum

	DFT (C-PCM in CH_2Cl_2)		experimental (in CH_2Cl_2)		
	E_{HOMO}	E_{LUMO}	E_{HOMO}[a]	E_{LUMO}[a]	$E_{Ex\ state}$[b]
1T	− 6.49	− 2.73	− 6.26[c]	− 2.68	− 3.16
2T	− 5.80	− 2.80	− 5.80	− 2.84	− 3.22
3T	− 5.38	− 2.84	− 5.54	− 2.93	− 3.23
4T	− 5.17	− 2.85	− 5.38	− 2.94	− 3.19
5T	− 4.98	− 2.86	− 5.27	− 2.96	− 3.15
P3HT	###	###	− 4.96	− 2.87[d]	− 3.08

[a]$E_{HOMO(LUMO)} = -4.88 - E_{OX(RED)}$. [b]$E_{Ex\ state} = E_{HOMO} + E_{gap}$ (optical). [c]Estimated HOMO value ($E_{HOMO} = E_{LUMO} - E_{gap}$ (optical) − $E_{Exciton}$). Exciton binding energy ($E_{Exciton}$) value was obtained by extrapolation of oligothiophene series (see the Supporting Information). [d]Estimated LUMO value ($E_{LUMO} = E_{HOMO} + E_{gap}$ (optical) + $E_{Exciton}$) assuming $E_{Exciton}$ = 0.2 eV by comparison with the oligothiophene series.

On the other hand, the difference between the calculated and experimental E_{HOMO} energies are much more severe. In this case, E_{HOMO} was overestimated by 0.4 eV for **1T**, well matched for **2T** and underestimated by 0.2 eV for **3T**, **4T**, and **5T**. However, the trend where a deeper E_{HOMO} is obtained upon reducing the number of thiophene units is clear and matches with our experimental values. Moreover, the orbital distribution is (de)localized over all thiophene units and consistent with the considerable shift of the E_{HOMO} (and as consequence in the energy gap) upon increasing the thiophene chain length, as observed in both electrochemical and optical measurements (Figures 2 and 4).

Table 2 also shows the experimental energy for the excited state (i.e., energy level from which photoinjection into TiO_2 would take place). These values were obtained using the optical gap rather than electrochemical gap to E_{HOMO} and thus take into account the exciton binding energy.[26,27] As expected, $E_{Ex\ state}$ energy values are deeper than E_{LUMO}.

3.4. TiO_2/P3HT Solar Cell Application. After having a complete picture of the molecular optical and electrochemical properties, we prepared a set of solar cells coupling oligothiophene functionalized mesoporous TiO_2 with P3HT, as described in the Experimental Section.

Device merit parameters and *J*−*V* curves are shown in Table 3 and Figure 6, respectively. We also report the merit parameters for a device prepared with neat TiO_2 (no oligothiophene), which shows power conversion efficiency (PCE) significantly lower than any of oligothiophene functionalized TiO_2 devices. In Table 3, we observe a strong increment in open circuit voltage (V_{OC}), which is proportional to the number of thiophene units present in the oligothiophene series. The V_{OC} is produced by the difference between the quasi-Fermi

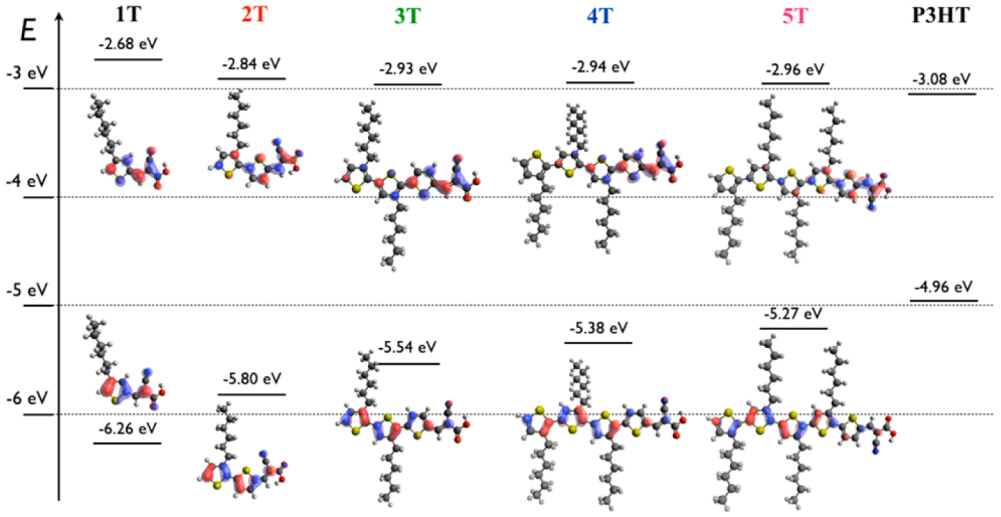

Figure 5. Molecular orbital distribution of HOMO (bottom) and LUMO (top) for oligothiophene series at B3LYP/6-31G(d) level of theory (isodensity = 0.04). Displayed HOMO and LUMO energy values are from experimental electrochemical measurements.

Table 3. Device Merit Parameters for Hybrid Solar Cells Prepared Using Oligothiophene-Functionalized TiO_2 and Undoped P3HT

	J_{SC} (mA cm^{-2})	PCE (%)	V_{OC} (V)	FF
neat TiO_2	0.23	0.04	0.46	0.39
1T	1.31	0.36	0.47	0.57
2T	0.53	0.17	0.60	0.53
3T	1.19	0.69	0.85	0.67
4T	1.23	0.79	0.88	0.72
5T	0.42	0.29	0.99	0.70

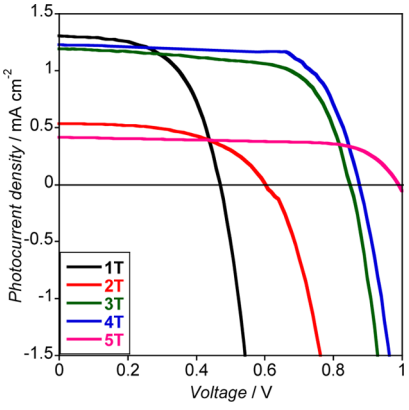

Figure 6. $J-V$ curves for hybrid solar cells prepared with oligothiophene-functionalized TiO_2 and undoped P3HT.

level for electrons in the TiO_2 and holes in the P3HT, which is strongly affected by any dipole generated between the TiO_2 and the P3HT and in particular from the dipole generated by molecules directly anchored at TiO_2 surface. The oligothiophene molecules resulted in a dipole moment pointing away from the TiO_2 surface, which spreads this energy offset and thus enhances the V_{OC}.[29] The intensity of this dipole is proportional to the number of thiophene units (see the Supporting Information), therefore a larger V_{OC} is expected with the increased number of thiophene units. Otherwise, the short circuit current density (J_{SC}) seems not to follow any particular trend with the number of thiophene units.

To estimate whether the photocurrent originates from light absorbed in oligothiophene or P3HT, we measured the external quantum efficiency (EQE) of the prepared devices, normalizing the spectra to the peak value between 450 and 750 nm (Figure 7). The oligothiophene molecules absorb light up to 500 nm

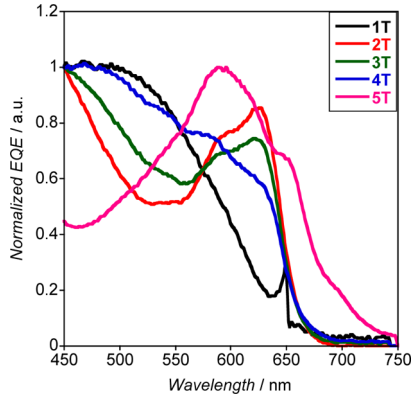

Figure 7. Normalized EQE for P3HT based ss-DSSC using oligothiophene series without dopant additives.

(depending on the number of thiophene units, see Figure 2), whereas the P3HT main absorption is localized over 550 nm (see the Supporting Information). In the EQE spectra in Figure 7, we can clearly distinguish the two contributions at lower and higher wavelength, because of oligothiophene and P3HT, respectively. The P3HT component becomes comparatively more pronounced than the oligothiophene upon increasing the number of thiophene units. In particular, for **5T**, we can clearly see that the P3HT dominates the EQE spectrum, with the typical absorption because of the stacking of the polymeric chains clearly visible at 650 nm.[17]

We prepared similar devices doping the P3HT with bis(trifluoromethanesulfonyl)imide (H-TFSI), which has been reported to improve the device performances in TiO_2 based solar cells.[22] Device merit parameters and $J-V$ curves for devices prepared using **5T** with and without H-TFSI are shown in Table 4 and Figure 8. We observe a 10-fold increment in J_{SC} and 200 mV lower V_{OC}. The latter can be explained considering that the addition of H-TFSI has been described in literature to

Table 4. Device Merit Parameters for P3HT-Based ss-DSSC Using 5T with and without H-TFSI

	J_{SC} (mA cm^{-2})	PCE (%)	V_{OC} (V)	FF
no additive	0.42	0.29	0.99	0.70
H-TFSI	4.65	2.32	0.79	0.63

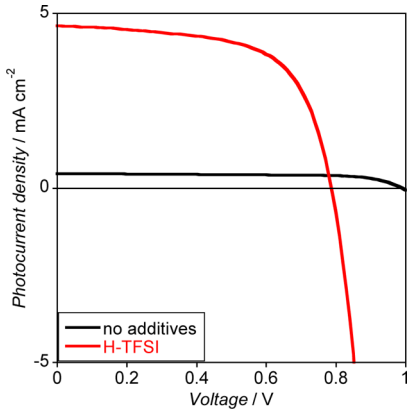

Figure 8. $J-V$ curves for P3HT based ss-DSSC using **5T** with (red line) and without (black line) H-TFSI additive.

cause negative shift of TiO_2 conduction band, which is consistent with the observed lowering in V_{OC}.[22]

From the EQE spectra in Figure 9, we see that in the H-TFSI doped device the photocurrent mainly originates from **5T**

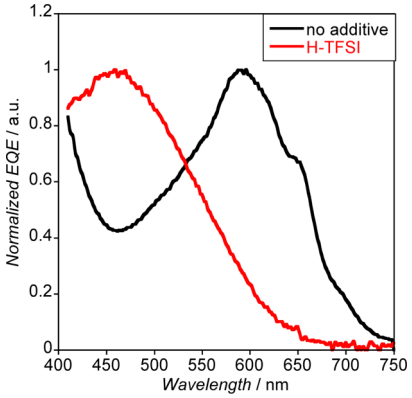

Figure 9. Normalized EQE for P3HT based ss-DSSC using **5T** with (red line) and without (black line) H-TFSI additive.

(absorption peak at 450 nm), with the P3HT contribution being comparative negligible. Doping the P3HT reduces the diffusion length of the photoexcited species (electron–hole pairs), which thus recombine before they can separate into free charges at TiO_2/P3HT interface, nullifying the P3HT contribution.[16]

Using H-TSFI with the other oligothiophenes, we observe a clear trend not only in V_{OC} as described above for devices without H-TFSI, but also for J_{SC} which increases with the number of thiophene units (Table 5 and Figure 10). Because the P3HT contribution to J_{SC} is nullified with H-TFSI (Figure 9), this increment of J_{SC} can be directly correlated to the oligothiophene absorption. Indeed, increasing the number of thiophene units, the oligothiophenes absorb a larger portion of the visible spectra, which allows for a larger photocurrent generation.

Table 5. Device Merit Parameters for P3HT ss-DSSC Using Oligothiophene Molecules with H-TFSI

	J_{SC} (mA cm^{-2})	PCE (%)	V_{OC} (V)	FF
1T	0.65	0.22	0.54	0.61
2T	0.67	0.23	0.59	0.57
3T	1.65	0.35	0.62	0.34
4T	4.41	1.54	0.69	0.50
5T	4.65	2.32	0.79	0.63

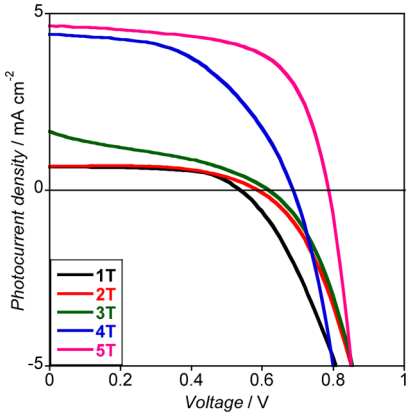

Figure 10. $J-V$ curves for P3HT ss-DSSC using oligothiophene series with H-TFSI.

In Figure 11, we propose a schematic representation of the oligothiophene energy levels relative to the P3HT, which justify the trend observed in device performances with and without the H-TFSI. In Figure 11, left, we reproduced the data reported in Figure 5, which showed that P3HT excited state level is below any of the oligothiophenes LUMO energy level. When the oligothiophenes are anchored on TiO_2, we need to consider that the effective LUMO levels are about 0.3 eV deeper (farther from the vacuum level) than the values measured in solution (Figure 11, middle).[23] With such a shift, the P3HT excited-state energy is positioned just below **1T**. This alignment explains the EQE spectrum for the **1T** device in Figure 7, which showed negligible P3HT contribution to the photocurrent, suggesting that **1T** is acting as an energetic barrier for the electron injection. Similarly, the EQE spectrum for the **5T** device suggests that the **5T** LUMO energy should be located below or in alignment with the TiO_2 conduction band, because no electron injection is allowed from **5T**. In Figure 11, right, we show that doping the P3HT with H-TFSI moves the TiO_2 conduction toward a more negative value, which enable charge injection also for **5T** but nullifies the P3HT contribution.

4. CONCLUSIONS

We have reported the synthesis and characterization of a series of conjugated 3-hexylthiophene derivatives (oligothiophenes) with a cyanoacrylic acid group, where we systematically increased the conjugation length from one up to five thiophene units. We studied their optoelectronic properties by UV–vis, PL and electrochemical methods, showing a lowering in LUMO energies together with energy gap reduction as the thiophene chain length increases from one to five thiophene units.

We used those oligothiophenes to functionalize TiO_2 nanoparticles, which we employed to prepare TiO_2/P3HT solar cells and study the effect of thiophene length on device

dx.doi.org/10.1021/am5050532 | ACS Appl. Mater. Interfaces 2014, 6, 17226–17235

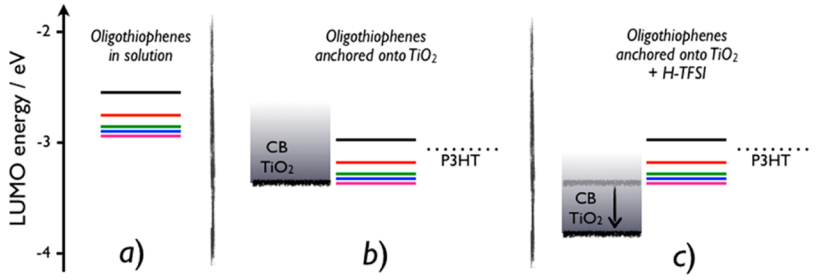

Figure 11. Schematic diagram of the oligothiophene LUMO energy levels: (a); in solution, anchored on TiO_2 without (b); and with H-TFSI doping (c); compared with the P3HT excited state energy level and the TiO_2 conduction band edge.

performances. EQE spectra showed that both oligothiophenes anchored on TiO_2 and P3HT can contribute to generate photocurrent. The P3HT contribution becomes comparatively more pronounced using oligothiophenes with increased number of thiophene units, but the overall device performances are significantly better with three or four thiophene units. We propose that a number of thiophene units lower or higher than three or four results in an energetic barrier for the charge extraction at the TiO_2/oligothiophene/P3HT interface. In particular, **1T** creates a barrier for charge collection from the P3HT, whereas **5T** cannot effectively inject into TiO_2. We also showed that doping the P3HT with H-TFSI enables a very effective charge extraction from all the oligothiophenes, but it nullifies the P3HT contribution. Hence, the use of a photoactive HTM such as P3HT, able to absorb light and transport holes, has a fundamental problem to its function. We only obtain significant photocurrent from doped devices, which mean that the device behaves as a solid state DSSC as the P3HT does not contribute to the photocurrent generation and therefore the use of a colorless HTM would be a better choice.

■ ASSOCIATED CONTENT

Supporting Information

^{1}H NMR spectra of **1** and **1T**. UV−visible spectra of **5T** at different concentrations. Cyclic voltammetry at different scan rates. Exciton binding energies vs thiophene units. Cyclic voltammetry and UV−visible spectrum of P3HT. Dipole moment vs thiophene units. This material is available free of charge via the Internet at http://pubs.acs.org/.

■ AUTHOR INFORMATION

Corresponding Authors

*E-mail: h.snaith1@physics.ox.ac.uk.
*E-mail: neil.robertson@ed.ac.uk

Author Contributions

†M.P. and A.A. contributed equally.

Notes

The authors declare no competing financial interest.

■ ACKNOWLEDGMENTS

We thank the Engineering and Physical Sciences Research Council (EPSRC) APEX project for financial support.

■ REFERENCES

(1) Dou, L.; You, J.; Hong, Z.; Xu, Z.; Li, G.; Street, R. A.; Yang, Y. 25th Anniversary Article: A Decade of Organic/Polymeric Photovoltaic Research. *Adv. Mater.* **2013**, *25*, 6642−6671.
(2) Hardin, B. E.; Snaith, H. J.; McGehee, M. D. The Renaissance of Dye-Sensitized Solar Cells. *Nat. Photonics* **2012**, *6*, 162−169.
(3) Graetzel, M.; Janssen, R. A.; Mitzi, D. B.; Sargent, E. H. Materials Interface Engineering for Solution-Processed Photovoltaics. *Nature* **2012**, *488*, 304−12.
(4) Mayer, A. C.; Scully, S. R.; Hardin, B. E.; Rowell, M. W.; McGehee, M. D. Polymer-Based Solar Cells. *Mater. Today* **2007**, *10*, 28−33.
(5) Kippelen, B.; Brédas, J.-L. Organic Photovoltaics. *Energy Environ. Sci.* **2009**, *2*, 251−261.
(6) Zhang, L.; Colella, N. S.; Cherniawski, B. P.; Mannsfeld, S. C.; Briseno, A. L. Oligothiophene Semiconductors: Synthesis, Characterization, and Applications for Organic Devices. *ACS Appl. Mater. Interfaces* **2014**, *6*, 5327−5343.
(7) Grancini, G.; Santosh Kumar, R. S.; Abrusci, A.; Yip, H.-L.; Li, C.-Z.; Jen, A.-K. Y.; Lanzani, G.; Snaith, H. J. Boosting Infrared Light Harvesting by Molecular Functionalization of Metal Oxide/Polymer Interfaces in Efficient Hybrid Solar Cells. *Adv. Funct. Mater.* **2012**, *22*, 2160−2166.
(8) Ren, S.; Chang, L. Y.; Lim, S. K.; Zhao, J.; Smith, M.; Zhao, N.; Bulović, V.; Bawendi, M.; Gradečak, S. Inorganic−Organic Hybrid Solar Cell: Bridging Quantum Dots to Conjugated Polymer Nanowires. *Nano Lett.* **2011**, *11*, 3998−4002.
(9) Jiang, K.-J.; Manseki, K.; Yu, Y.-H.; Masaki, N.; Suzuki, K.; Song, Y.-l.; Yanagida, S. Photovoltaics Based on Hybridization of Effective Dye-Sensitized Titanium Oxide and Hole-Conductive Polymer P3HT. *Adv. Funct. Mater.* **2009**, *19*, 2481−2485.
(10) Zhu, R.; Jiang, C.-Y.; Liu, B.; Ramakrishna, S. Highly Efficient Nanoporous TiO2-Polythiophene Hybrid Solar Cells Based on Interfacial Modification Using a Metal-Free Organic Dye. *Adv. Mater.* **2009**, *21*, 994−1000.
(11) Coakley, K. M.; Liu, Y.; McGehee, M. D.; Frindell, K. L.; Stucky, G. D. Infiltrating Semiconducting Polymers into Self-Assembled Mesoporous Titania Films for Photovoltaic Applications. *Adv. Funct. Mater.* **2003**, *13*, 301−306.
(12) Abrusci, A.; Ding, I. K.; Al-Hashimi, M.; Segal-Peretz, T.; McGehee, M. D.; Heeney, M.; Frey, G. L.; Snaith, H. J. Facile Infiltration of Semiconducting Polymer into Mesoporous Electrodes for Hybrid Solar Cells. *Energy Environ. Sci.* **2011**, *4*, 3051−3058.
(13) Liu, J.; Tanaka, T.; Sivula, K.; Alivisatos, A. P.; Fréchet, J. M. J. Employing End-Functional Polythiophene to Control the Morphology of Nanocrystal-Polymer Composites in Hybrid Solar Cells. *J. Am. Chem. Soc.* **2004**, *126*, 6550−6551.
(14) Lin, Y.-Y.; Chu, T.-H.; Li, S.-S.; Chuang, C.-H.; Chang, C.-H.; Su, W.-F.; Chang, C.-P.; Chu, M.-W.; Chen, C.-W. Interfacial Nanostructuring on the Performance of Polymer/TiO2 Nanorod Bulk Heterojunction Solar Cells. *J. Am. Chem. Soc.* **2009**, *131*, 3644−3649.
(15) Liu, J.; Kadnikova, E. N.; Liu, Y.; McGehee, M. D.; Fréchet, J. M. J. Polythiophene Containing Thermally Removable Solubilizing Groups Enhances the Interface and the Performance of Polymer-Titania Hybrid Solar Cells. *J. Am. Chem. Soc.* **2004**, *126*, 9486−9487.
(16) Abrusci, A.; Santosh Kumar, R. S.; Al-Hashimi, M.; Heeney, M.; Petrozza, A.; Snaith, H. J. Influence of Ion Induced Local Coulomb Field and Polarity on Charge Generation and Efficiency in Poly(3-Hexylthiophene)-Based Solid-State Dye-Sensitized Solar Cells. *Adv. Funct. Mater.* **2011**, *21*, 2571−2579.

(17) Canesi, E. V.; Binda, M.; Abate, A.; Guarnera, S.; Moretti, L.; D'Innocenzo, V.; Sai Santosh Kumar, R.; Bertarelli, C.; Abrusci, A.; Snaith, H.; Calloni, A.; Brambilla, A.; Ciccacci, F.; Aghion, S.; Moia, F.; Ferragut, R.; Melis, C.; Malloci, G.; Mattoni, A.; Lanzani, G.; Petrozza, A. The Effect of Selective Interactions at the Interface of Polymer−Oxide Hybrid Solar Cells. *Energy Environ. Sci.* **2012**, *5*, 9068−9076.
(18) Boon, F.; Thomas, A.; Clavel, G.; Moerman, D.; De Winter, J.; Laurencin, D.; Coulembier, O.; Dubois, P.; Gerbaux, P.; Lazzaroni, R. Synthesis and Characterization of Carboxystyryl End-Functionalized Poly (3-hexylthiophene)/TiO2 Hybrids in View of Photovoltaic Applications. *Synth. Met.* **2012**, *162*, 1615−1622.
(19) Cossi, M.; Rega, N.; Scalmani, G.; Barone, V. Energies, Structures, and Electronic Properties of Molecules in Solution with the C-PCM Solvation Model. *J. Comput. Chem.* **2003**, *24*, 669−681.
(20) Frisch, M. J.; Trucks, G. W.; Schlegel, H. B.; Scuseria, G. E.; Robb, M. A.; Cheeseman, J. R.; Scalmani, G.; Barone, V.; Mennucci, B.; Petersson, G. A.; Nakatsuji, H.; Caricato, M.; Li, X.; Hratchian, H. P.; Izmaylov, A. F.; Bloino, J.; Zheng, G.; Sonnenberg, J. L.; Hada, M.; Ehara, M.; Toyota, K.; Fukuda, R.; Hasegawa, J.; Ishida, M.; Nakajima, T.; Honda, Y.; Kitao, O.; Nakai, H.; Vreven, T.; Montgomery, J. A., Jr.; Peralta, J. E.; Ogliaro, F.; Bearpark, M.; Heyd, J. J.; Brothers, E.; Kudin, K. N.; Staroverov, V. N.; Kobayashi, R.; Normand, J.; Raghavachari, K.; Rendell, A.; Burant, J. C.; Iyengar, S. S.; Tomasi, J.; Cossi, M.; Rega, N.; Millam, J. M.; Klene, M.; Knox, J. E.; Cross, J. B.; Bakken, V.; Adamo, C.; Jaramillo, J.; Gomperts, R.; Stratmann, R. E.; Yazyev, O.; Austin, A. J.; Cammi, R.; Pomelli, C.; Ochterski, J. W.; Martin, R. L.; Morokuma, K.; Zakrzewski, V. G.; Voth, G. A.; Salvador, P.; Dannenberg, J. J.; Dapprich, S.; Daniels, A. D.; Farkas, O.; Foresman, J. B.; Ortiz, J. V.; Cioslowski, J.; Fox, D. J. *Gaussian 09*, revision B.01; Gaussian, Inc.: Wallingford, CT, 2009.
(21) Hanwell, M.; Curtis, D.; Lonie, D.; Vandermeersch, T.; Zurek, E.; Hutchison, G. Avogadro: an Advanced Semantic Chemical Editor, Visualization, and Analysis Platform. *J. Cheminform.* **2012**, *4*, 17.
(22) Abate, A.; Hollman, D. J.; Teuscher, J.; Pathak, S.; Avolio, R.; D'Errico, G.; Vitiello, G.; Fantacci, S.; Snaith, H. J. Protic Ionic Liquids as p-Dopant for Organic Hole Transporting Materials and their Application in High Efficiency Hybrid Solar Cells. *J. Am. Chem. Soc.* **2013**, *135*, 13538−13548.
(23) Planells, M.; Abate, A.; Hollman, D. J.; Stranks, S. D.; Bharti, V.; Gaur, J.; Mohanty, D.; Chand, S.; Snaith, H. J.; Robertson, N. Diacetylene Bridged Triphenylamines as Hole Transport Materials for Solid State Dye Sensitized Solar Cells. *J. Mater. Chem. A* **2013**, *1*, 6949−6960.
(24) Snaith, H. J. How Should You Measure Your Excitonic Solar Cells? *Energy Environ. Sci.* **2012**, *5*, 6513−6520.
(25) Kanemitsu, Y.; Suzuki, K.; Tomiuchi, Y.; Shiraishi, Y.; Kuroda, M.; Nabeta, O. Luminescence from Oligothiophenes and Thiophene-Based Oligomers. *Synth. Met.* **1995**, *71*, 2209−2210.
(26) Inamdar, S. N.; Ingole, P. P.; Haram, S. K. Determination of Band Structure Parameters and the Quasi-Particle Gap of CdSe Quantum Dots by Cyclic Voltammetry. *ChemPhysChem* **2008**, *9*, 2574−2579.
(27) Knupfer, M. Exciton Binding Energies in Organic Semiconductors. *Appl. Phys. A: Mater. Sci. Process.* **2003**, *77*, 623−626.
(28) Jones, B. A.; Facchetti, A.; Wasielewski, M. R.; Marks, T. J. Tuning Orbital Energetics in Arylene Diimide Semiconductors. Materials Design for Ambient Stability of n-Type Charge Transport. *J. Am. Chem. Soc.* **2007**, *129*, 15259−15278.
(29) Cappel, U. B.; Plogmaker, S.; Johansson, E. M.; Hagfeldt, A.; Boschloo, G.; Rensmo, H. Energy Alignment and Surface Dipoles of Rylene Dyes Adsorbed to TiO2 Nanoparticles. *Phys. Chem. Chem. Phys.* **2011**, *13*, 14767−14774.